International Journal of Pharmacy and Pharmaceutical Research (IJPPR)
Volume 30, Issue 12, December 2024 **ijppr.humanjournals.com** ISSN: 2349-7203

Green Synthesis of Nickel Nanoparticles from Leaf Extracts of *Ocimum sanctum* for Antimicrobial Activities

Km Anjali Gupta*, Prof. Pawan Kumar Jain, Mr. Narendra Singh

Shri Ramnath Singh Mahavidyalaya (Pharmacy), Gormi, Bhind, M.P., India

Received: 2024-12-10 Revised: 2024-12-20 Accepted: 2024-12-27

ABSTRACT

The field of nanotechnology is the most active area of research in modern materials science. Though there are many chemicals as well as physical methods, green synthesis of nanomaterials is the most emerging method of synthesis. We report the synthesis of nickel nanoparticles (Ni-Gs) using leaf broth of medicinal herb, *Ocimum sanctum* (Tulsi). The synthesized Ni-Gs have been characterized by UV-Vis spectroscopy, transmission electron microscopy (TEM), and X-ray diffractometry. The mean particle of synthesized Ni-Gs was found to be 12- 36 nm, as confirmed by TEM. The qualitative assessment of reducing potential of leaf extract has also been carried out which indicated presence of significant amount of reducing entities. FTIR analysis play dual role of reducing and stabilizing agent of nanoparticles in aqueous solution. Such Ni-Gs stabilized by Tulsi leaf extract were found to have enhanced antimicrobial activity against well-known pathogenic strains, namely Staphylococcus aureus and E. coli.

KEYWORDS: Nanotechnology, Nickel, Nanoparticle, Ocimum sanctum, Antimicrobial activity

INTRODUCTION

Nanoparticles find extensive biological and nonbiological [1,2] applications due to their unique physical and chemical properties, distinct morphology, size, shape, crystalline nature, surface area-to-volume ratio, electro-optical, magneto-optical, chemical and mechanical properties [3]. They can be synthesized by hydrothermal, microemulsion, electrospray, coprecipitation, laser ablation and sol-gel processes. However, these approaches are quite expensive, low yielding and involve toxic chemicals which pose a threat to the environment [5]. Now, the trend is shifting towards the green synthesis of NPs in the presence of plant extracts, microorganisms and enzymes. Green synthesis of NPs is attracting the attention of scientists and researchers due to its rapid, cost-effective, ecofriendly and sustainable approach [6]. The plant extract acts as a capping agent through a coordination action by capturing the metal ions in the amylose helix on well-defined sites [7]. The texture of plant leaves and petals acts as a bio template and thereby controls the size of the nanoparticles and hinders the agglomeration of particles.

Among all metal nanoparticles, nickel nanoparticles attract unlimited attention in the field of nanotechnology due to their unique properties such as chemical stability, good conductivity, catalytic, and most importantly antibacterial, antiviral, antifungal [9]. Generally, nickel nanoparticles are synthesized using various techniques to obtain different shapes and sizes for use in various applications. Various chemical and physical preparation methods are used to produce nanoparticles, including radiation, chemical precipitation, photochemical methods, electrochemical, and Langmuir-Blodgett techniques [10]. The use of chemical and physical method in the synthesis of nanoparticles is very expensive and cumbersome and leads to the presence of some toxic chemicals that are absorbed on the surface and may have adverse effects on applications, so there is an increasing need to develop environmentally benign nanoparticles. Biosynthetic methods using microorganisms or plant extracts have emerged as a simple and viable alternative to chemical synthetic procedures and physical methods [11].

Green synthesis of nanoparticles using plant extracts, due to their easy accessibility, is emerging as an important research topic in the field of bionanotechnology today [12]. The synthesis of nanoparticles by means of plants is simpler and easier compared to typical physical and chemical methods as it can be studied without any special operating conditions. Synthesized products of the process, including waste products, are derived from natural plant extracts and thus this technique is highly environmentally friendly. With the bio-based nanoparticle synthesis protocol, higher reproducibility of the process and higher stability of the synthesized nanoparticles can be achieved. Therefore, the bio-based production of nanoparticles is suitable for large-scale production that is more effective cost investment, environmentally friendly and safe for human therapeutic use [13].

In this context, to the best of our knowledge, the green synthesis of Ni-Gs with *Ocimum sanctum* leaves is still not reported. For this purpose, the synthesis of nickel nanoparticles with the reducing properties of molecules such as terpenoids found in the extract of Ocimum sanctum was carried out. Current studies were performed to produce Ni-Gs in *Ocimum* sanctum leaves. [14] Some of the main advantages of green synthesis of Ni-Gs are excellent yield, short duration, simplicity, environmental sustainability, green chemical reaction, and cost-effectiveness. Their structural features were compared by spectroscopic, microscopic and thermometric techniques including FTIR, Raman, XRD, SEM, TGA and DSC. [15] The synthesized Ni-Gs were subjected to antimicrobial activity were determined.

MATERIALS AND METHODS

Preparation of leaves sample and Chemicals: The fresh leaves of *O. sanctum* was washed thoroughly under running tap water followed by distilled water. The washed leaves were shade dried at 37 °C for 3 days, powdered by grinding and then sieved using a 15-mesh sieve. The obtained leaf powder was used for the extraction. All the solvents used for this study were of analytical reagent grade and purchased from Merck, Mumbai.

Figure 1: Tulsi Leaves

Preparation of *Ocimum sanctum* leaf extracts: About 250 gm of leaf powder was extracted in Soxhlet apparatus using different solvents such as petroleum ether, chloroform, ethyl acetate, ethanol and water (aqueous) in the order of increasing polarity. [16] Rotary vacuum evaporator was used to concentrate each extract. The obtained extracts with each solvent were accurately weighed and the percentage of yield was calculated in terms of dry weight of the leaf powder.

Synthesis of nickel nanoparticles (Ni-Gs): Ni-Gs was synthesized by treating 10 mL of aqueous leaf extracts of *O. sanctum* with 1 mM/L of aqueous nickel nitrate ($Ni(NO_3)_2$) solution by vigorous stirring for 3 h at 60 °C. The obtained Ni-Gs was purified by repeated centrifugation at 5000 rpm for 15 min and then re- dispersion in deionized water. The contents were then freeze-dried for 24 h to obtain dry powder of nanoparticles. The resulting nanoparticles powder was stored at 4 °C until further use. [17]

Characterization of Ni-Gs:

1. UV–Vis Spectroscopy: UV–Vis spectroscopy is based on the amount of light absorbed due to electronic transitions in samples and the absorption mainly depends on the particle size and chemical surroundings. The metal nanoparticles exhibits high extinction coefficient and their surface plasmon property are shape and size dependent. Therefore, the formation of nanoparticles could be detected by UV–Vis spectroscopy. In the present study, the absorbance of Ni-Gs was recorded using Shimadzu UV-2401 PC double beam spectrometer in the wavelength range of 300–600 nm at 37 °C. [18]

2. Fourier Transform Infrared Spectroscopy: FTIR is based on the atomic vibrations in a molecule and the infrared (IR) spectrum of nanoparticles is obtained by passing IR radiations through the sample and evaluating the amount of incident radiation that were absorbed at a specific frequency. Thus, the frequencies of IR radiation absorbed (peaks) in FTIR directly correlate to the bonds present within the sample. FTIR analysis of Ni-Gs was carried out by applying 1 mg of Ni-Gs in 100 mg KBr at 0.25 mm thickness and stabilized in a reactive humidity prior to acquiring the spectrum using FTIR spectrometer (Nicolet 380). The spectrum was then analyzed for 32 scans between 500 and 4000 nm. [19]

3. X–ray Diffraction: In the present study, the XRD analysis of synthesized Ni-Gs was performed using XPERT-PRO, PANalytical diffractometer system equipped with Ni-filtered Cu K-α1 radiation (k = 0.15406 nm) with scanning range (2θ) of 10°–80° at 37 °C with a step size of 0.05° 2θ and step time of 10.1 s. [20] The average crystallite domain size (D) of Ni-Gs which is perpendicular to the reflecting planes was determined from the width of XRD peaks using the Scherrer equation represented by the following equation:

$$D = 0.94 \lambda / \beta \cos \theta$$

Where, λ is the X–ray wavelength, θ is the diffraction angle and β is the full width at half maximum (FWHM).

4. Thermo-gravimetric (TG) analysis: Thermo-gravimetric (TG) analysis is used to study the thermal stability of the material and the fraction of its volatile components by observing the change in weight which occurs on heating the sample. Changes observed in the mass of the sample at elevated temperature are due to rupture of various bonds that result in evolution of volatile products. In the present study, thermal stability of Ni-Gs was carried out by TG analysis (Shimadzu TGA-Q500 instrument) in nitrogen atmosphere (50 mL/min) by heating 5 mg of sample from 37 °C to 550 °C at the rate of 10 ϵC/min. [21]

5. Differential Scanning Calorimetry (DSC): DSC analysis was used to evaluate the phase transformation of nanoparticles based on change in heat flow (temperature) to the sample and standard. In this study, DSC analyzer (Shimadzu DSC-50, Japan) with 10 µW detection sensitivity was used to study the phase transformation in Ni-Gs. The up-going positive peaks and down-moving negative peaks were measured as exothermic and endothermic processes respectively. [22]

6. Antimicrobial Assay: Antibacterial and antifungal assays were performed with Muller Hinton (MH) agar and Sabouraud dextrose (SD) agar medium respectively. Microbial cultures were prepared to 0.5 McFarland standards prior to the assay. Antimicrobial activity of Ni-Gs was evaluated by disc diffusion assay against the Gram−negative bacteria (*E. coli* (MTCC 1682), *K. pneumoniae* (MTCC 8911), *S. typhi* (MTCC 3224)) and Gram−positive bacteria (*B. subtilis* (MTCC 6133), *S. epidermidis* (MTCC 7919)). Antifungal activity was also tested against fungal pathogens such as *C. albicans* (MTCC 3018), *C. tropicalis* (MTCC 6222), *A. fumigatus* (MTCC 2508), *A. clavatus* (MTCC 1323) and *A. niger* (MTCC 281). Pure microbial cultures were subcultured and uniformly swabbed on individual plates. [23] 20 µl of Ni-Gs at different concentrations (25, 50, 100 µg/mL) were impregnated to 6 mm filter paper discs, dried and placed on the culture plate. Bacterial and fungal cultures were incubated at 37 °C for 24 h and 48 h respectively. Antimicrobial activities were studied by measuring the diameter of the zone of inhibition. Deionized water (as control) and leaf extracts were used to compare the antimicrobial activity of Ni-Gs. [24]

i) Minimum inhibitory concentration (MIC), Minimum bactericidal concentration (MBC) and Minimum fungicidal concentration (MFC) assay: The MIC of control, antibiotics and Ni-Gs was determined 100 µL of Ni-Gs in serially diluted from 200 to 1 µg/mL were added to microtitre plates with 100 µL MH broth for bacterial samples or 100 µL SD broth for fungal samples. Two−fold serial dilution was performed and 100 µL of bacterial and fungal samples were inoculated to the respective wells. Bacterial and fungal plates were incubated for 24 h and 48 h respectively at 37 ºC and optical densities were determined at 600 nm using microplate reader. Antibiotics (amoxicillin (Amx) and nystatin (Nys) were used to compare the bactericidal and fungicidal activity of Ni-Gs. MBC and MFC were determined by subculturing 2 µL of above MIC serial diluted sample after 24 h of incubation in respective wells containing 100 µL of MH or SD broth/well. [25] Number of bacterial and fungal colonies was counted after incubation for 24 h and 48 h respectively at 37 ºC. MBC and MFC was the lowest concentration of nanoparticles or antibiotics that prevented the growth of bacterial and fungal colonies on solid media. [26]

ii) Analysis of microbial growth kinetics: Microbial growth rate was observed by inoculating the microtitre plates with MH and SD broth containing 10^5 CFU/mL of bacterial or fungal pathogens respectively and loaded with varied concentrations of nanoparticles (25, 50 and 100 µg/mL). The plates were incubated at 37 °C and shaken at 180 rpm. [27, 28, 29] After inoculation, the optical density (OD) at 600 nm (Sondi and Sondi 2004) was serially monitored at every 3 h interval till 24 h and every 6 h interval till 48 h for bacterial and fungal pathogens respectively.

RESULTS AND DISCUSSION

Green Synthesis of Nickel Nano Particles: Ni-Gs was synthesized using nickel nitrate as precursor and aqueous leaf extracts of *O. sanctum* as reducing agent. Nickel nitrate in aqueous solution dissociates into Ni^{2+} and nitrate ions. The hydrated electrons from *O. sanctum* leaf extracts reduce Ni^{2+} into zero valent nickel (Ni^0) nanoparticles by nucleation process. Few Ni^0 atoms agglomerate to form Ni^0_n which is due to the binding energy between two metal atoms as for silver nanoparticles (AgO_2) and for nickel nanoparticles ($Ni0_2$).

International Journal of Pharmacy and Pharmaceutical Research (IJPPR)
Volume 30, Issue 12, December 2024 ijppr.humanjournals.com ISSN: 2349-7203

Characterization of Ni-Gs:

1. UV–Vis Spectroscopy: UV–Vis absorbance spectrum of Ni-Gs showed maximum absorbance at 395 nm. UV–Vis spectroscopy curves and surface plasmon resonance (SPR) wavelength were sensitive to the characteristics of nanoparticles and the absorption spectra at 374 to 422 nm range corresponds to the SPR of nickel. Related to this study, the presence of absorption peak at 395 nm shows the presence of nickel nanoparticles. The maximum wavelength and width of the SPR are mainly dependent of the size and shape of the nanoparticles. The broadness of the bandwidth indicates the size of the nanoparticles. Therefore, increased bandwidth evidenced the presence of smaller particle size of nanoparticles.

2. Fourier Transform Infrared Spectroscopy: FTIR analysis was performed to identify the biomolecules involved in capping and stabilizing the synthesized Ni-Gs. FTIR spectrum of Ni-Gs bands at 3163 cm^{-1}, 2348 cm^{-1}, 2282 cm^{-1}, 1638 cm^{-1}, 1401 cm^{-1}, 1122 cm^{-1} and 723 cm^{-1} that corresponds to O–H stretching vibration of carboxylic acids, C–N stretching vibration, C–C triple bonds, N–H vibration of amide linkages, C–C stretch (in ring) in aromatics, C–N stretching vibrations of amines and C–H rock in alkanes respectively. FTIR spectra of Ni-Gs evidenced the presence of proteins and amide linkages which is in concurrence with for silver nanoparticles. FTIR analysis of Ni-Gs confirmed the presence of O–H, N–H, C–N, and C–H functional groups. These functional groups and proteins were found to act both as capping and stabilizing Ni-Gs for nanoparticles have also shown that the carbonyl groups of peptides, amino acid residues and free amine groups in the proteins have the ability to bind with the metal nanoparticles.

3. X–ray diffraction: The XRD spectrum of Ni-Gs showed five distinct diffraction peaks at 2θ values of 37.32°, 44.82°, 47.92°, 63.11° and 72.97° with maximum peak intensity at 44.82° and their miller indices (111) and (200) confirmed the face-centered-cubic (fcc) structure of nickel. The XRD pattern of Ni-Gs correlates with the Joint Committee on Powder Diffraction Standards database (JCPDS PDF No.: 04 – 0850) that evidenced random powdered arrangement for nickel. The average particle size of Ni-Gs calculated using equation (3.7) was found to be 30 nm. These results are in concurrence with for chemical synthesized nickel nanoparticles. Peak broadening in XRD spectra evidenced the formation of smaller sized Ni-Gs for nanoparticles. Therefore, the XRD analysis of synthesized Ni-Gs evidenced for fcc crystal structure of Ni-Gs with particle size of 30 nm.

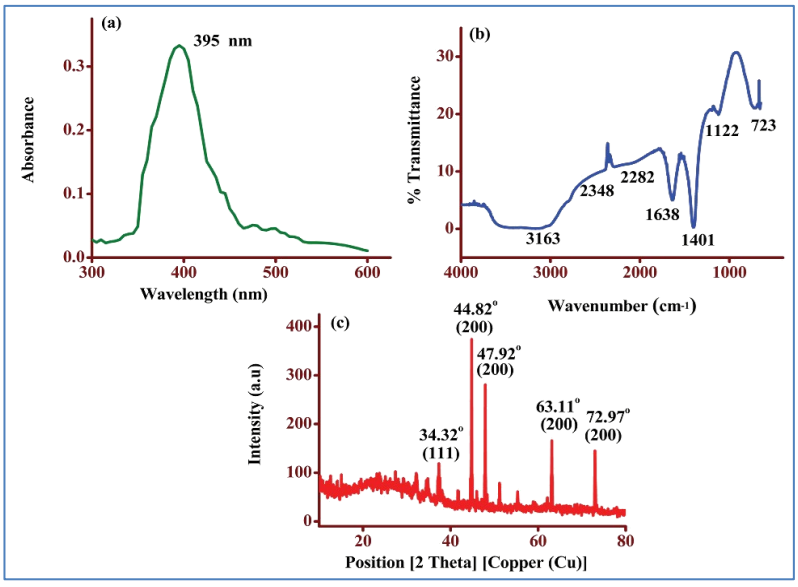

Figure 2: (a) UV–Visible spectrum, (b) FTIR spectrum and (c) XRD pattern of Ni-Gs. The characterization of Ni-Gs evidenced maximum absorbance at 395 nm, existence of O–H, N–H, C–N, C–H functional groups and face centered cubic structure of nickel.

4. Thermo-gravimetric (TG) Analysis: Thermogravimetric (TG) curves of Ni-Gs showed few stabilizing and destabilizing interaction in accordance with the temperature region. Two major weight losses were observed in Ni-Gs between 100–300 ºC and 350–410 ºC. The second major weight loss of 25 % occurred at 350 ºC. Above 490 °C, there was no further weight loss of Ni-Gs and constant weight was observed. The minor and major weight loss of Ni-Gs could be attributed to the decomposition of adsorbed biomolecules, thermal dehydration of nanoparticles and organic residues respectively for nickel chloride nanoparticles. the decomposition of nickel carbonate could result in weight loss near 300 ºC in TG curve of nickel oxide nanoparticles.

International Journal of Pharmacy and Pharmaceutical Research (IJPPR)
Volume 30, Issue 12, December 2024 ijppr.humanjournals.com ISSN: 2349-7203

5. Differential Scanning Calorimetry (DSC): In DSC analysis, the oxidation of nanoparticles during heating and its stability was evidenced from DSC thermogram. Exothermic peak at 350 °C was observed on heating Ni-Gs at rate of 10 °C. This is attributed to the weight loss occurring as a result of oxidation of nanoparticles at higher temperatures for metal nanoparticles. The exothermic peak at 350 ºC for Ni-Gs could be due to the decomposition of biomolecules coating nanoparticles and is in concurrence with for iron oxide nanoparticles. Therefore, oxidative stability of Ni-Gs depends on the capping or surrounding biomolecules.

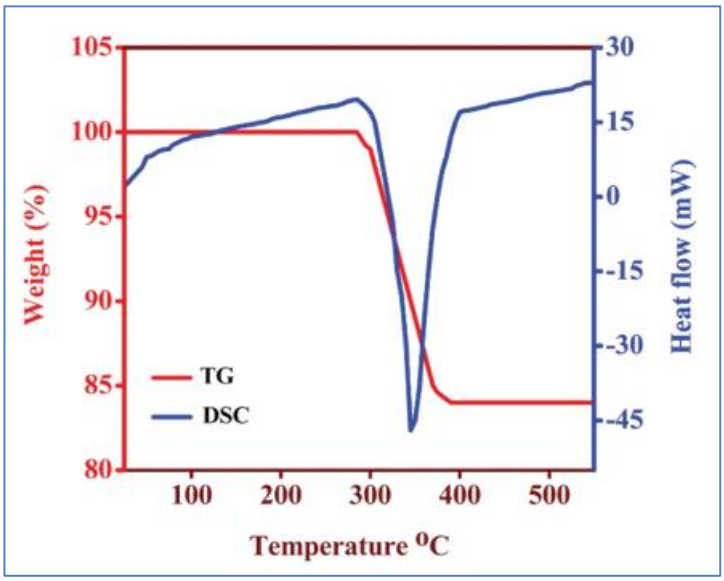

Figure 3: TG curve and DSC thermogram of Ni-Gs. The TG curve (red) showing weight loss in temperature ranges of 100–300 ºC and 350–410 ºC when heated upto 550ºC at heating rate of 10 ºC/min. DSC thermogram (blue) evidenced exothermic peak at 350 ºC.

Antibacterial and Antifungal Activity of Ni-Gs: In disc diffusion assay, the suppression of bacterial growth was determined in petriplates loaded with 25−100 µg/mL Ni-Gs after 24 h at 37 ºC. Zone of inhibition was not observed in control plates loaded with deionized water while leaf extracts showed higher growth inhibition. 25−100 µg/mL of Ni-Gs showed inhibition zone of 15.3−25.1 mm, 9.5−23.3 mm, 8−20.2 mm, 7.1−19.5 mm and 5.2−18.6 mm in *E. coli, K. pneumoniae, S. typhi, B. subtilis* and *S. epidermidis* respectively.

Table 1: Zone of inhibition (mm) of Ni-Gs against bacterial and fungal pathogens.

1. Zone of inhibition (mm)				
2. Bacterial/ Fungal Pathogens	**3. Leaf extracts (50 µg/mL)**	**4. Ni-Gs (µg/mL)**		
		5. 25	**6. 50**	**7. 100**
8. E. coli	9. 9.0 ± 0.2	10. 15.3 ± 0.3	11. 19.2 ± 0.5	12. 25.1 ± 0.1
13. K. pneumoniae	14. 7.8 ± 0.9	15. 9.5 ± 0.5	16. 18.1 ± 0.7	17. 23.3 ± 0.7
18. S. typhi	19. 5.8 ± 0.3	20. 8.0 ± 1.4	21. 18.3 ± 0.3	22. 20.2 ± 0.3
23. B. subtilis	24. 5.2 ± 0.5	25. 7.1 ± 0.8	26. 16.5 ± 0.2	27. 19.5 ± 0.5
28. S. epidermidis	29. 3.9 ± 0.6	30. 5.2 ± 0.3	31. 16.0 ± 0.8	32. 18.6 ± 0.9
33. C. albicans	34. 7.8 ± 0.1	35. 14.5 ± 0.4	36. 18.2 ± 0.7	37. 23.1 ± 0.4
38. C. tropicalis	39. 5.2 ± 0.6	40. 12.4 ± 0.8	41. 14.4 ± 0.2	42. 21.6 ± 0.9
43. A. clavatus	44. 4.5 ± 0.3	45. 10.4 ± 0.1	46. 14.3 ± 0.1	47. 18.7 ± 0.5
48. A. fumigatus	49. 3.7 ± 0.4	50. 8.5 ± 0.3	51. 10.7 ± 0.9	52. 15.5 ± 0.6
53. A. niger	54. 2.5 ± 0.1	55. 6.2 ± 0.5	56. 7.5 ± 0.5	57. 12.4 ± 0.1

Data represent mean values of triplicate experiments ± standard deviation (SD).

The size of inhibition zone increases linearly with increase in Ni-Gs concentration (25−100 µg/mL). The presence of inhibition zone in Figure 4 confirmed the antifungal activity of Ni-Gs. The size of inhibition zone differed with the type of fungal pathogen and the concentration of Ni-Gs. Maximum antifungal activity was observed at 100 µg/mL of Ni-Gs for *C. albicans* (23.1 mm), *C. tropicalis* (21.6 mm), *A. clavus* (18.7 mm), *A. fumigatus* (15.5 mm) and *A. niger* (12.4 mm).

International Journal of Pharmacy and Pharmaceutical Research (IJPPR)
Volume 30, Issue 12, December 2024 ijppr.humanjournals.com ISSN: 2349-7203

Zone of inhibition was not observed in plates loaded with deionized water for tested fungal pathogens. Leaf extracts showed minimal antifungal activity with diameter of inhibition zone as 7.8, 5.2, 4.5, 3.7 and 2.5 mm for *C. albicans, C. tropicalis, A. clavatus, A. fumigatus* and *A. niger* respectively. Maximum antimicrobial activity was observed at 100 µg/mL of Ni-Gs for all tested pathogens than at lower concentrations (25, 50 µg/mL).

Data evidenced dose dependent antimicrobial activity of Ni-Gs with maximum inhibition at 100 µg/mL. This is due to the release of nickel ions from Ni-Gs that damages the membrane permeability leading to cell death. This observation is in good agreement with the antibacterial activity of zinc oxide nanoparticles at 2−12 mM concentration and for silver nanoparticles at concentration of 10−150 µM.

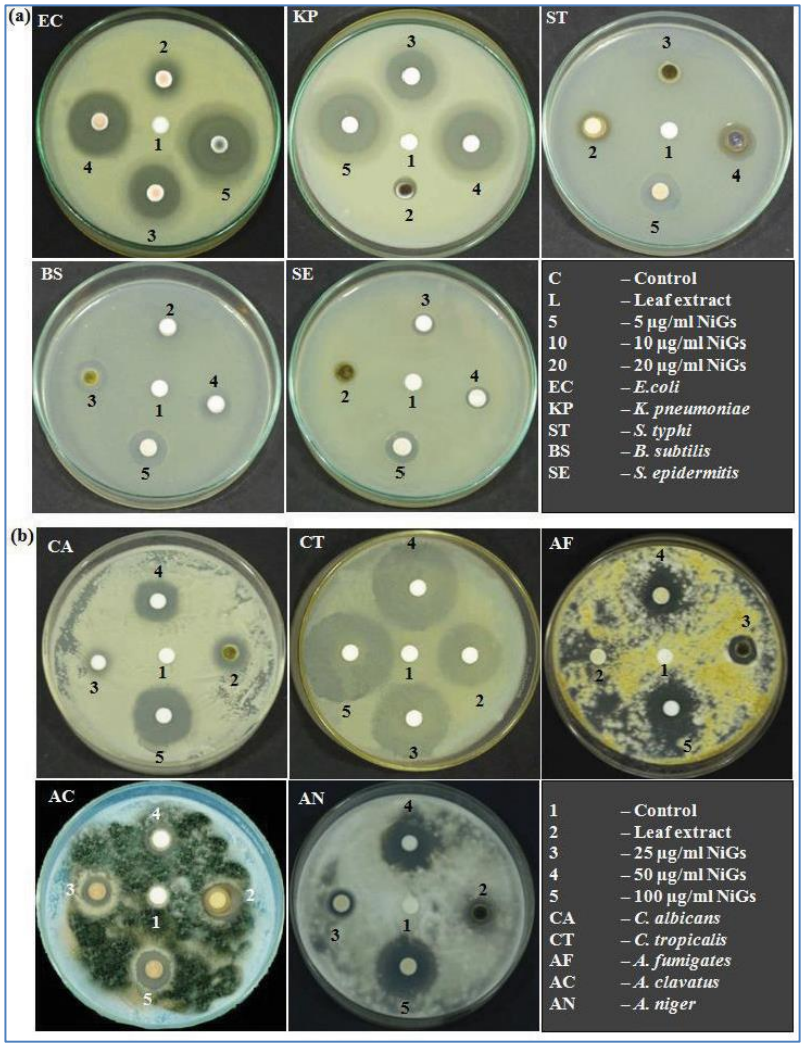

Figure 4: Zone of inhibition of (a) bacteria and (b) fungi treated with Ni-Gs.

Minimum Inhibitory Concentration (MIC) and Minimum Microbicidal Concentration (MBC/MFC): MIC of Ni-Gs was studied to determine the lowest concentration that could completely inhibit visible growth of bacterial and fungal pathogens. Antimicrobial activity of Ni-Gs in terms of MIC, MBC and MFC is shown in Table 2. Both inhibitory and bactericidal concentration of leaf extracts was found to be 100 µg/mL for Gram−positive bacteria (*B. subtilis* and *S.epidermidis*) and Aspergillus species (*A. clavatus, A. fumigatus* and *A. niger*) while 50 µg/mL was observed for Gram−negative bacteria (*E. coli, K. pneumonia* and *S. typhi*) and *Candida species* (*C. albicans and C. tropicalis*). 25 µg/mL Ni-Gs was the minimum inhibitory concentration against all bacterial pathogens. 25 µg/mL Ni-Gs showed bactericidal activity against *E. coli, K. pneumonia* and *S. typhi* while 50 µg/mL Ni-Gs exhibited bactericidal activity against *B. subtilis* and *S. epidermidis*. This data is comparable with the antibiotic amoxicillin which showed 50 µg/mL of MIC for all tested bacterial pathogens and 100 µg/mL of MBC for *S. typhi, B. subtilis* and *S. epidermidis*. 25 µg/mL of amoxicillin showed bactericidal activity against *E. coli, K. pneumoniae, S. typhi, B. subtilis* and *S. epidermidis*. Therefore, the MIC (25 µg/mL) and MBC (50 µg/mL) of Ni-Gs was much lower than the tested antibiotics.

International Journal of Pharmacy and Pharmaceutical Research (IJPPR)
Volume 30, Issue 12, December 2024 **ijppr.humanjournals.com** ISSN: 2349-7203

Among the fungal pathogens tested, maximum sensitivity was observed in *C. albicans, C. tropicalis* that showed MIC and MFC of Ni-Gs at 25 and 50 µg/mL respectively. MIC and MFC of Ni-Gs was found to be 50 µg/mL for *A. clavatus, A. fumigatus and A. niger*. MIC and MFC of antibiotic nystatin was observed at 50 and100 µg/mL for most of the fungal pathogens tested. *B. subtilis, S. epidermidis, A. clavatus, A. fumigatus* and *A. niger* has showed MIC, MBC and MFC of Ni-Gs at 50 µg/mL.

Table 2: MIC, MBC and MFC of Ni-Gs against bacterial and fungal pathogens.

58. Bacterial/ Fungal Pathogens	**59. Leaf extracts**		**60. Antibiotics (µg/mL)**		**61. Ni-Gs (µg/mL)**	
	62. MIC	**63. MBC/MFC**	**64. MIC**	**65. MBC/MFC**	**66. MIC**	**67. MBC/MFC**
68. E. coli	69. 50 ± 0.3	70. 50 ± 0.1	71. 25 ± 0.3	72. 50 ± 1.3	73. 25 ± 0.3	74. 25 ± 2.4
75. K. pneumoniae	76. 50 ± 0.1	77. 50 ± 0.2	78. 50 ± 2.0	79. 50 ± 0.1	80. 25 ± 2.8	81. 25 ± 0.7
82. S. typhi	83. 50 ± 1.0	84. 100 ± 0.8	85. 50 ± 0.4	86. 100 ± 0.0	87. 25 ± 0.2	88. 25 ± 1.6
89. B. subtilis	90. 100 ± 0.5	91. 100 ± 1.3	92. 50 ± 1.7	93. 100 ± 0.2	94. 50 ± 0.2	95. 50 ± 0.2
96. S. epidermidis	97. 100 ± 0.2	98. 100 ± 0.6	99. 50 ± 0.2	100. 100 ± 0.1	101. 50 ± 0.5	102. 50 ± 0.1
103. C. albicans	104. 50 ±0.2	105. 50 ± 0.4	106.50 ±0.1	107. 50 ± 2.1	108. 25 ± 1.4	109. 50 ± 0.0
110. C. tropicalis	111. 50 ± 0.1	112. 100 ± 0.1	113. 50 ± 0.7	114.100 ± 0.8	115. 25 ± 0.7	116.50 ± 0.1
117. A. clavatus	118. 100 ± 2.5	119. 100 ± 0.9	120. 50 ± 0.0	121.100 ± 1.2	122. 50 ± 2.5	123.50 ± 0.5
124. A. fumigatus	125. 100 ± 0.0	126. 100 ± 1.3	127. 100 ± 0.3	128.100 ± 0.0	129. 50 ± 1.0	130.50 ± 1.2
131. A. niger	132. 100± 0.9	133. 100 ± 0.2	134. 100 ± 1.0	135.100 ± 0.3	136. 50 ± 0.8	137.50 ± 0.6

Data represent mean values of triplicate experiments ± standard deviation (SD).

But Gram−negative bacteria, *C. albicans* and *C. tropicalis* has showed higher sensitivity to Ni-Gs at lower concentration (25 µg/mL). *S. typhi* and *C. tropicalis* recorded higher MBC and MFC (100 µg/mL) respectively for both leaf extracts and antibiotics. Higher antimicrobial activity was observed in Ni-Gs than antibiotics and leaf extracts for all the tested pathogens. No significant antibacterial and antifungal activity was observed at Ni-Gs concentration less than 25 µg/mL. Gram−negative bacteria and Candida species showed relatively higher sensitivity to all tested antimicrobial agents (Ni-Gs, antibiotics and leaf extracts) than Gram−positive bacteria and Aspergillus species respectively. It is clear from the results that Ni-Gs have enhanced inhibitory, bactericidal and fungicidal activities.

Higher MIC and MBC values of Ni-Gs in Gram−positive (*B. subtilis* and *S. epidermidis*) pathogens than in Gram−negative bacteria (*E. coli, K. pneumonia and S. typhi*) is due to thick peptidoglycan layer in Gram−positive bacteria that prevented the easy penetration of nanoparticles through the cell membrane. Similarly, Selvaraj et al. (2014) have also reported higher MIC values of green synthesized silver nanoparticles (25 µg/mL) against Gram−positive bacteria than Gram−negative bacteria (6.25 µg/mL). Higher MIC and MFC values of Ni-Gs in *A. clavatus, A. fumigatus* and *A. niger* than in *C. albicans* and *C. tropicalis* is due to spore producing and filamentous nature of Aspergillus species *(A. clavatus, A. fumigatus* and *A. niger*) which decreased its sensitivity to Ni-Gs. This observation for antimicrobial properties of biosynthesized silver nanoparticles against *S. aureus, S. epidermidis, E. coli, A. niger* and *C. albicans*. Enhanced MIC, MBC and MFC of Ni-Gs than antibiotics and leaf extracts are due to its larger surface to volume ratio and its penetration to cell membrane. This observation is in concurrence with the for antimicrobial activity against of silver nanoparticles activity against *C. albicans* and *E. coli* respectively.

The antimicrobial activity (MIC) of Ni-Gs was compared with the antimicrobial studies of silver nanoparticles (Table 3) reported in literature. Ni-Gs showed better antimicrobial activity when compared to silver nanoparticles of similar particle size. This result evidenced for higher antimicrobial activity of Ni-Gs than silver nanoparticles. Also, the variations in antimicrobial activity of Ni-Gs than silver nanoparticles of similar size are attributed to the differences in experimental conditions, shape and crystal structure of the nanoparticles. Therefore, the antimicrobial effectiveness of green synthesized metal nanoparticles depends on particle dosage, treatment time and synthesis methods. This observation is in concurrence for green synthesized zinc oxide nanoparticles.

International Journal of Pharmacy and Pharmaceutical Research (IJPPR)
Volume 30, Issue 12, December 2024 ijppr.humanjournals.com ISSN: 2349-7203

Table 3: Comparison of antimicrobial activity of Ni-Gs with silver nanoparticles.

138. Bacterial/ Fungal Pathogens		139. MIC in µg/mL			
		140. 141.	Ni-Gs (12–36 nm)	142. 143.	Silver nanoparticles (Size in nm)
144.	*E. coli*	145.	25	146.	75 (21 nm)
147.	*K. pneumoniae*	148.	25	149.	11 (11–75 nm)
150.	*S. typhi*	151.	25	152.	75 (21 nm)
153.	*B. subtilis*	154.	50	155.	70 (20 nm)
156.	*S. epidermidis*	157.	50	158.	31.25 (10–50 nm)
159.	*C. albicans*	160.	25	161.	500 (10–30 nm)
162.	*C. tropicalis*	163.	25	164.	840 (25 nm)
165.	*Aspergillus sp.*	166.	50	167.	40 (18 nm)
168.	*A. fumigatus*	169.	50	170.	8 (20 nm)
171.	*A. niger*	172.	50	173.	75 (20 nm)

Growth curves of microbial cells treated with different concentrations of Ni-Gs Bacterial growth curves (Figure 5) clearly demonstrated the inhibition of bacterial growth at all tested concentrations of Ni-Gs (25−100 µg/mL). Culture medium without Ni-Gs has not shown any inhibition of growth and also reached stationary phase after 24 h. However, complete inhibition was obtained at 50 and 100 µg/mL of Ni-Gs for both Gram−positive (*B. subtilis and S. epidermidis*) and Gram−negative bacteria (*E. coli, K. pneumonia and S. typhi*). 25 µg/mL of Ni-Gs had slightly inhibited the growth of bacteria but was not sufficient to outpace the reproduction of bacterial cells.

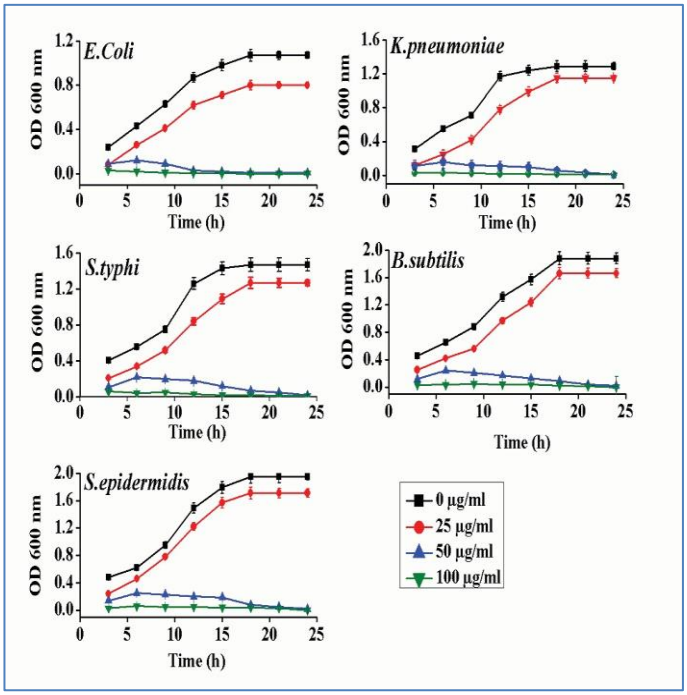

Figure 5: Bacterial growth curves after exposure to varied Ni-Gs concentrations. Untreated microbial samples were used as control. The error bars represent standard error.

From the results, it is evidenced that the bactericidal activity of Ni-Gs increased with increasing Ni-Gs concentration. Ni-Gs has showed faster inhibition of growth in *E. coli*, *K. pneumonia* and *S. typhi* than in *B. subtilis* and *S. epidermidis*. Maximum inhibition was observed in E. coli at 100 µg/mL of Ni-Gs. Inhibitory effects of Ni-Gs on the growth and reproduction of fungal pathogens with respect to Ni-Gs concentration is shown in the Fig. 6. In the absence of Ni-Gs, growth of both tested Candida species (*C. albicans* and *C. tropicalis*) and Aspergillus species (*A. clavatus, A. fumigatus* and *A. niger*) reached exponential phase rapidly. However when exposed to 25 µg/mL of Ni-Gs, growth lagged for longer hours (9 h and 24 h for bacterial and fungal pathogens respectively).

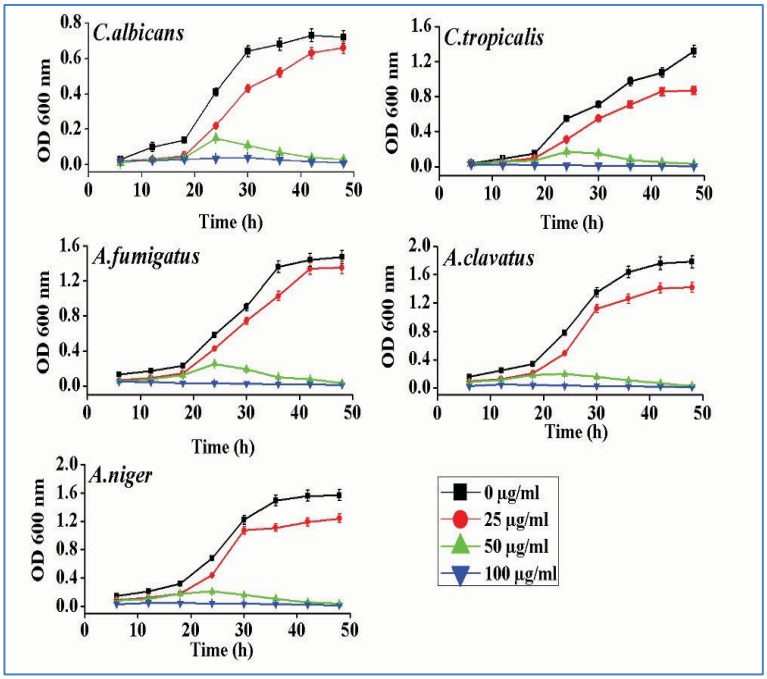

Figure 6: Fungal growth curves after exposure to varied Ni-Gs concentrations. Untreated microbial samples were used as control. The error bars represent standard error.

Further increasing Ni-Gs concentration to 50 µg/mL suppressed the fungal growth while 100 µg/mL of Ni-Gs completely inhibited the growth of fungal pathogens. 100 µg/mL of Ni-Gs showed maximum inhibition in *C. albicans* while the effect was much less at lower concentrations (25, 50 µg/mL). Therefore, the complete growth inhibition of bacterial and fungal pathogens was at 50 µg/mL and 100 µg/mL of Ni-Gs respectively. Faster inhibition of growth and reproduction of bacterial and fungal pathogens at 100 µg/mL than 25 and 50 µg/mL Ni-Gs is due to the decrease in the availability of nanoparticles for inhibition. Decreased antimicrobial activity at lower Ni-Gs concentration is due to the availability of few Ni-Gs for growth inhibition for antibacterial activities of metallic oxide (ZnO, MgO and CaO) powders against *S. aureus* and *E. coli*. Microbicidal activity of Ni-Gs is also due to the electrostatic interaction between positively charged nickel ions with negatively charged microbial cell membranes. These observations are in concurrence for antimicrobial activity of zinc oxide nanoparticles against *S. enterica* and *C. albicans*.

CONCLUSION

Therefore, the presence of these phytochemicals at higher concentrations in aqueous and ethanolic *O. sanctum* leaf extracts could play major role in medical applications. The UV−Vis spectrum of Ni-Gs evidenced maximum absorbance peak at 395 nm. FTIR spectrum of Ni-Gs exhibited peaks characteristic for functional groups such as N−H, C−N, C−H and O−H. XRD pattern evidenced fcc crystal structure of Ni-Gs. SEM and TEM analysis of Ni-Gs evidenced that the morphology of Ni-Gs was almost spherical with 12−36 nm in size. TG and DSC analysis of Ni-Gs showed good thermal stability. Therefore, this simple and economical green synthesis of nickel nanoparticles can be used as an alternative to physical, chemical and microbial mediated methods. Gram−negative bacteria (*E. coli, K. pneumonia* and *S. typhi*) and Candida species (*C. albicans, C. tropicalis*) showed higher growth inhibition and microbicidal activity when treated with Ni-Gs than Gram−positive bacteria (B. subtilis and S. epidermidis) and Aspergillus species (*A. clavatus, A. fumigatus and A. niger*) respectively. Enhanced antimicrobial activity of Ni-Gs was attributed to the leakage of cellular proteins, reducing sugar, respiratory dehydrogenase and DNA efflux through damaged cell membrane resulting in cell death. This study reveals the potential application of Ni-Gs as an antimicrobial agent at concentration of 50 µg/mL and hence can be used as antimicrobial coatings on the surface of materials for various environmental and biomedical applications.

REFERENCES

1. Nosheen S, Irfan M, Abidi SH, et al. A review: development of magnetic nano vectors for biomedical applications. GSC Adv Res Rev. 2021;8:85–110.
2. Mueez A, Hussain S, Ahmad M, et al. Green synthesis of nanosilver particles from plants extract. Int J Agric Env Biores. 2022;7:96–122.

3. Hussain S, Amjad M. A review on gold nanoparticles (GNPs) and their advancement in cancer therapy. Int J Nanomater Nanotechnol Nanomed. 2021;7:19–25.
4. Rahman MA, Radhakrishnan R, Gopalakrishnan R. Structural, optical, magnetic and antibacterial properties ofNd doped NiO nanoparticles prepared by co-precipitation method. J Alloys Compd. 2018;742:421–429.
5. Jia F, Zhang L, Shang X, et al. Non-aqueous Sol–Gel approach towards the controllable synthesis of nickel nanospheres, nanowires, and nanoflowers. Adv Mater. 2008;20:1050–1054.
6. Nagaraj B, Krishnamurthy N, Liny P, et al. Biosynthesis of gold nanoparticles of Ixora coccinea flower extract & their antimicrobial activities. Int J Pharma Bio Sci. 2011;2:557–565.
7. Deshpande K, Mukasyan A, Varma A. Direct synthesis of iron oxide nanopowders by the combustion approach: reaction mechanism and properties. Chem Mater. 2004;16:4896–4904.
8. Sana SS, Singh RP, Sharma M, et al. Biogenesis and application of nickel nanoparticles: a review. Curr Pharm Biotechnol. 2021;22:808–822.
9. J. Lee, S. Mahendra, P.J. Alvarez, Nanomaterials in the construction industry: are view of their applications and environmental health and safety considerations, ACS Nano 4 (7) (2010) 3580–3590.
10. B. Kim, C.S. Park, M. Murayama, M.F. Hochella Jr., Discovery and characterization of silver sulfide nanoparticles in final sewage sludge products, Environ. Sci. Technol. 44 (19) (2010) 7509–7514.
11. A. Mehta, M. Sharma, A. Kumar, S. Basu, Effect of Au content on the enhanced photocatalytic efficiency of mesoporous Au/TiO2 nanocomposites in UV and sunlight, Gold Bull. 50 (1) (2017) 33–41.
12. A. Mehta, A. Mishra, M. Sharma, S. Singh, S. Basu, Effect of silica/titania ratio on enhanced photooxidation of industrial hazardous materials by microwave treated mesoporous SBA-15/TiO2 nanocomposites, J. Nanoparticle Res. 18 (7) (2016) 209.
13. H. A. Salam, R.Sivaraj, VenckateshR ,Green synthesis and characterization of zinc oxide Nanoparticles from Ocimumbasilicum L. var. purpurascensBenth.-Lamiaceae leaf extract,Mater. Lett., https://doi.org/10.1016/j.matlet.2014.05.033.
14. Rameshthangam, P., & Chitra, J. P. (2018). Synergistic anticancer effect of green synthesized nickel nanoparticles and quercetin extracted from Ocimum sanctum leaf extract. Journal of materials science & technology, 34(3), 508-522.
15. Asmathunisha, N., & Kathiresan, K. (2013). A review on biosynthesis of nanoparticles by marine organisms. Colloids and Surfaces B: Biointerfaces, 103, 283-287.
16. Fardood, S. T., Ramazani, A., & Moradi, S. (2017). A novel green synthesis of nickel oxide nanoparticles using Arabic gum. Chemistry Journal of Moldova, 12(1), 115-118.
17. Kasthuri, J., Veerapandian, S., & Rajendiran, N. (2009). Biological synthesis of silver and gold nanoparticles using apiin as reducing agent. Colloids and Surfaces B: Biointerfaces, 68(1), 55-60.
18. Ezhilarasi, A. A., Vijaya, J. J., Kaviyarasu, K., Kennedy, L. J., Ramalingam, R. J., & Al-Lohedan, H. A. (2018). Green synthesis of NiO nanoparticles using Aegle marmelos leaf extract for the evaluation of in-vitro cytotoxicity, antibacterial and photocatalytic properties. Journal of Photochemistry and Photobiology B: Biology, 180, 39-50.
19. Huang, J., Li, Q., Sun, D., Lu, Y., Su, Y., Yang, X., ... & Chen, C. (2007). Biosynthesis of silver and gold nanoparticles by novel sundried Cinnamomum camphora leaf. Nanotechnology, 18(10), 105104.).
20. Govindasamy, R., Jeyaraman, R., Kadarkaraithangam, J., Arumugam, M., Gandhi, E., Chinnaperumal, K., Thirunavukkarasu, S., Sampath, M., Abdul, A, Z., Asokan, B., Chidambaram, J., Arivarasan, V.K., Moorthy, I, Chinnadurai, S., "Novel and simple approach using synthesized nickel nanoparticles to control blood-sucking parasites", Vet. Parasitol. 191, 332□339 (2013).
21. Wang, X, S., Liu, X., Wen, L., Zhou, Y., Li, Z., "Comparison of basic dye crystal violet from aqueous solution by low-cost biosorbents", Sep. Sci. Technol., 43, 3712–3731 (2008).
22. Shahla, E., Maryam, A., Ladan, E., "Preparation and characterization of Diethylentriamine -montmorillonite and its application for removal of Eosin Y dye: Optimization, kinetic and isotherms study", J. Sci. Ind. Res., 72, 461–466 (2013).
23. Uzaire, R., Arun, I., Abida, K., "Synthesis, characterization and application of nanomaterials for the removal of emerging pollutants from industrial waste water, kinetics and equilibrium model", J. Water Sustain., 2, 233-244 (2012).
24. Ahmed, R., "Studies on adsorption of crystal violet from aqueous solution onto coniferous pinus bark powder", J. Hazard. Mater., 171, 767□773 (2009).
25. El-Sayed., "Removal of methylene blue and crystal violet from aqueous solutions by palm kernel fiber", Desalination., 272, 225–232 (2011).
26. A.L. Brandt, A. Castillo, K.B. Harris, J.T. Keeton, M.D. Hardin, T.M. Taylor, Inhibition of Listeria monocytogenes by Food Antimicrobials Applied Singly and in Combination, J Food Sci 75(9) (2010) M557-M563.
27. Brandt, A. L., Castillo, A., Harris, K. B., Keeton, J. T., Hardin, M. D., & Taylor, T. M. (2010). Inhibition of Listeria monocytogenes by food antimicrobials applied singly and in combination. Journal of Food Science, 75(9), M557-M563.
28. Pang, H., Lu, Q., Chen, C., Liu, X., & Gao, F. (2011). Facile synthesis of Ni 3 (BO 3) 2 nanoribbons and their antimicrobial, electrochemical and electrical properties. Journal of Materials Chemistry, 21(36), 13889-13894.
29. Chaudhary, R. G., Tanna, J. A., Gandhare, N. V., Rai, A. R., & Juneja, H. D. (2015). Synthesis of nickel nanoparticles: Microscopic investigation, an efficient catalyst and effective antibacterial activity. Adv. Mater. Lett, 6(11), 990-998.

International Journal of Pharmacy and Pharmaceutical Research (IJPPR)
Volume 30, Issue 12, December 2024 **ijppr.humanjournals.com** ISSN: 2349-7203

How to cite this article:
Km Anjali Gupta et al. Ijppr.Human, 2024; Vol. 30 (12): 300-310.

Conflict of Interest Statement: All authors have nothing else to disclose.